

DOI: 10.1002/cphc.201402146

Probing Protonation Sites of Isolated Flavins Using IR Spectroscopy: From Lumichrome to the Cofactor Flavin Mononucleotide

Judith Langer,^[a] Alan Günther,^[a] Sophie Seidenbecher,^[a] Giel Berden,^[b] Jos Oomens,^[b, c] and Otto Dopfer^{*[a]}

Infrared spectra of the isolated protonated flavin molecules lumichrome, lumiflavin, riboflavin (vitamin B₂), and the biologically important cofactor flavin mononucleotide are measured in the fingerprint region (600–1850 cm⁻¹) by means of IR multiple-photon dissociation (IRMPD) spectroscopy. Using density functional theory calculations, the geometries, relative energies, and linear IR absorption spectra of several low-energy isomers are calculated. Comparison of the calculated IR spectra with the measured IRMPD spectra reveals that the N10 substituent on the isoalloxazine ring influences the protonation

site of the flavin. Lumichrome, with a hydrogen substituent, is only stable as the N1-protonated tautomer and protonates at N5 of the pyrazine ring. The presence of the ribityl unit in riboflavin leads to protonation at N1 of the pyrimidinedione moiety, and methyl substitution in lumiflavin stabilizes the tautomer that is protonated at O2. In contrast, flavin mononucleotide exists as both the O2- and N1-protonated tautomers. The frequencies and relative intensities of the two C=O stretch vibrations in protonated flavins serve as reliable indicators for their protonation site.

1. Introduction

Flavins play an important role in many biochemical reactions as cofactors in flavoproteins and as blue-light-sensitive units in photoreceptors.^[1–4] The most prominent flavins are lumiflavin (LF), riboflavin (RF), flavin mononucleotide (FMN), and flavin adenine dinucleotide (FAD). RF, also known as vitamin B₂ or lactoflavin, is found in many different types of food. Deficiency of this vitamin in humans causes growth retardation, skin disease, and hair loss. Light-induced reactions of blue-light photoreceptors are controlled by photophysical and photochemical processes of flavins, for example, FMN binding to light-oxygen-voltage-sensing (LOV) domain in phototropin in the signaling state.^[5,6] As versatile cofactors, FAD and FMN are further involved in a variety of enzymatic reactions and are able to mediate one- or two-electron reactions.^[7–9] For this purpose, fla-

vins can exist in three different oxidation states, namely the oxidized, radical, and reduced forms.

All flavins contain a 7,8-dimethyl-substituted isoalloxazine chromophore, which consists of benzene (I), pyrazine (II), and pyrimidinedione (III) units with different functional groups (R) at position N10 (Figure 1). LC (without N10 substituent) exists

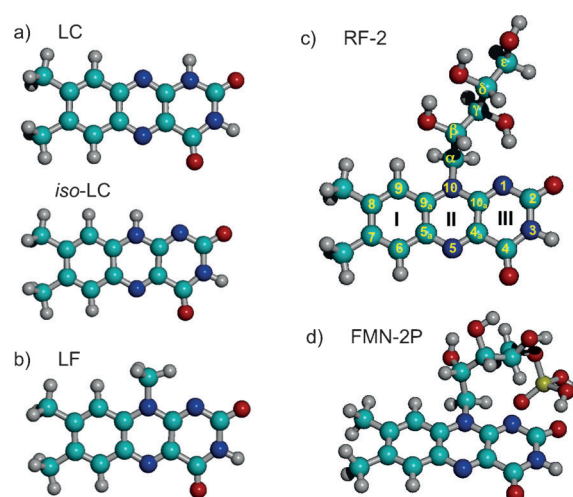


Figure 1. Structures of flavins considered in this study. They consist of a 7,8-dimethylisoalloxazine skeleton and differ in the substituent R attached to N10: a) R = H in lumichrome (LC and iso-LC), b) R = CH₃ in lumiflavin (LF), c) R = ribityl in riboflavin (RF), and d) R = ribophosphate in flavin mononucleotide (FMN). LC occurs in two tautomeric forms, namely alloxazine (LC) or isoalloxazine (iso-LC). The numbering of the aromatic system conforms to IUPAC, and the Greek letter notation in the ribityl side chain of RF is used to discriminate possible conformers.

[a] Dr. J. Langer,^{*} A. Günther, S. Seidenbecher, Prof. Dr. O. Dopfer
Technische Universität Berlin, Institut für Optik und Atomare Physik
Hardenbergstraße 36, D-10623 Berlin (Germany)
E-mail: dopfer@physik.tu-berlin.de

[b] Dr. G. Berden, Prof. Dr. J. Oomens
Radboud University Nijmegen, Institute for Molecules and Materials
FELIX Facility
Toernooiveld 7, 6525 ED Nijmegen (The Netherlands)

[c] Prof. Dr. J. Oomens
University of Amsterdam
Science Park 904, 1098 XH Amsterdam (The Netherlands)

[†] Current address:
Parque Tecnológico de San Sebastian
Paseo Miramon 182, Edif C
20009 San Sebastian (Spain)

Supporting Information for this article is available on the WWW under
<http://dx.doi.org/10.1002/cphc.201402146>.

in two tautomeric forms (Figure 1a), namely alloxazine (LC, protonated at N1) and isoalloxazine (iso-LC, protonated at N10). The thermodynamically stable alloxazine form can tautomerize to the metastable isoalloxazine by proton transfer in the excited state.^[10–12] LF does not tautomerize in this way, due to the presence of the methyl substituent at N10, which stabilizes the isoalloxazine form (Figure 1b). In RF and FMN, the methyl group is replaced by ribityl and ribophosphate, respectively (Figure 1c and d). Both compounds are not photostable and exposure to light leads to their decay into LF and LC as photoproducts. The aromatic ring structure of flavins is planar^[13–17] in the oxidized state and usually bent about the N5–N10 axis in the reduced state.^[18,19] Calculations suggest that the bending is not a result of steric hindrance but of electronic preferences.^[20] Therefore, the bending angle regulates the delocalized electron density in the ring system^[21] and thus the redox properties of flavins. The redox chemistry is basically restricted to the chromophore but the reaction equilibria depend on the substituent R, which strongly affects the electronic structure of the flavin.

In order to understand the relation between structure and reactivity of flavins and flavoproteins, extensive spectroscopic studies on dynamics, electronic structure, and vibrational properties have been performed in solution and solid pellets by means of NMR spectroscopy,^[22] ESR spectroscopy,^[23] optical dynamic discrimination,^[24] UV absorption and fluorescence spectroscopy,^[25–27] Stark spectroscopy,^[28] ultrafast-IR spectroscopy,^[29–31] Raman spectroscopy,^[32,33] and far-IR spectroscopy.^[34] Environmental factors, such as solvation (solvatochromism),^[35] pH, polarity, buffer, and ionic strength can affect the geometrical, vibrational, and electronic structure, and consequently the reactivity of flavins, resulting in energy shifts of electronically excited states, lifetime changes, and the stabilization of different redox and protonation states.^[3]

The flavin redox potential can be modulated by modification of the solvent (protic or aprotic) or by specific binding to a protein site. In addition, subtle fine-tuning of the redox potential range occurs through the formation of different types of H-bonds,^[36] π -stacking interactions with the flavin nucleus,^[37] and conformational changes.^[38] The flavin chromophore offers five positions that can be involved in H-bonding, namely N1, N5, N3, C2=O, and C4=O. In this respect, the carbonyl groups

C2=O and C4=O play a crucial role as electron donors. An empirical linear relationship between the C=O stretch frequency ($\nu_{\text{C=O}}$) and the C=O bond length ($R_{\text{C=O}}$),^[39] as well as a correlation between the C=O stretch frequency shift $\Delta\nu_{\text{C=O}}$ and the H-bond enthalpy ΔH , has been determined.^[40–42] H-bonding to C4=O lowers the energy of the LUMO orbital resulting in activation of a hydride transfer to the N5 position.^[43] Kim and Carey observed a blueshift of the C4=O stretch vibration in RF bound to a protein compared to the free species in aqueous solution.^[44] They concluded that the H-bond between C4=O and the protein residue is weaker than that between C4=O and water molecules of the solvent. Furthermore, Hazegawa et al. found a linear relationship between the increase of $R_{\text{C4=O}}$ and the enhancement of electron density at C4 by correlating

the Raman frequency redshift of the C4=O stretch mode with the chemical shift of the ¹³C NMR signal upon H-bonding for several free flavins in solution and those bound to flavoproteins.^[19] They assumed that the H-bond enhances the electrophilic character of the neighboring N5 position.

In previous studies, the theoretical treatment of isolated flavin molecules has not always properly reproduced the available experimental data in solution or solid state due to the neglect of environmental effects. At the same time, much effort has been made to adapt theoretical concepts for isolated molecules to solvated species in order to interpret more accurately the spectroscopic results, for example, as a function of the dielectric constant of the solvent.^[45,46] A recent calculation of IR spectra of flavins in aqueous solution using a combination of density functional theory (DFT) with molecular mechanics predicts large $\Delta\nu_{\text{C2=O}}$ and $\Delta\nu_{\text{C4=O}}$ shifts of about 50 cm⁻¹, inhomogeneous vibrational band broadening, and intensity changes.^[47] The latter effect can be explained by the increase of the C=O dipole moments upon water solvation.

Depending on the pH value of the solvent, flavins can appear in the anionic (deprotonated), neutral, or cationic (protonated) state.^[48,49] Significant shifts of the absorption wavelength and changes of fluorescence quantum yields indicate that (de)protonation of the ring system also strongly influences the electronic properties.^[50] Zheng and Ornstein investigated theoretically the three oxidation states of LF molecules in their available protonation states using the Hartree–Fock (HF) method.^[13] They found that the oxidized form exhibits a planar structure due to electron delocalization over the three rings. In addition, the planarity is independent of the protonation state, H-bonding, protein environment, and crystal packing forces.^[13] The N5 position can principally act as an electrophilic^[21] or nucleophilic site, can be protonated, or can form an H-bond with donor groups of the protein or solvents. Two isomers of protonated LF^[13] were considered. The first one is protonated at N1 and the second one at N5. The N1-protonated species is energetically favored by 79 kJ mol⁻¹ and has a slightly pyramidal N1 center. In contrast, the N5 center is planar in the N5-protonated species. In order to classify flavoproteins, Wouters et al. determined the geometry, charge distribution, and HOMO–LUMO topologies of protonated flavins in different redox states using the HF/3-21G level of theory.^[51] They concluded that a larger electron delocalization, as demonstrated by a smaller bond length alternation upon protonation, as well as a larger basicity associated with a more negative charge, can explain the favorable protonation at N1 with respect to N5 and also the unusual electrophilic affinity of N5 when LF is protonated at N1. On the other hand, Meyer et al. have used semi-empirical and ab initio methods [HF and second-order Møller–Plesset electron correlation theory (MP2)] to predict the relative energies of oxidation and protonation states.^[52] They found that the O2-protonated tautomer is more stable than the N1 species in the gas phase. By applying self-consistent reaction field (SCRf) calculations, the authors also demonstrated that the energy gap between O2- and N1-protonated tautomers becomes much smaller when the molecule is embedded in a polar medium.

In order to understand the influence of the environment on the structure and stabilization of flavins at a molecular level, it is necessary to study experimentally the intrinsic structure and reactivity of isolated flavin molecules in different protonation states. The only available spectroscopic study of flavins in the gas phase deals with two-color pump-probe UV photodissociation (UVPD) of protonated FMN.^[53] The authors observed that UVPD of protonated FMN leads to decomposition into protonated LC and LF, while the collision-induced process shows completely different dissociation channels, namely the loss of H₂O and H₃PO₄. The branching ratio between protonated LC and LF changes significantly when an IR probe pulse is applied after electronic excitation. To identify the intrinsic structure of isolated molecules, IRMPD spectra of mass-selected ions generated in an electrospray ionization (ESI) source can be measured, which, in combination with theoretical calculations, allow the isomeric structures to be determined. In the past decade, this approach has extensively been applied for the investigation of the structures (including low-energy conformers) of a variety of biomolecular ions, for example, DNA mononucleotides, DNA bases, amino acids, peptides, drugs and drug-receptor molecules.^[54–61] As a proof-of-concept for the class of flavins, we report here the first IRMPD spectra of protonated LC, LF, RF and FMN combined with the computational analysis of different isomers including conformers. In order to discuss the effect of protonation on the geometry, vibrational structure, and energetics, we also compare the calculated spectra of the neutral and the corresponding protonated species. This study represents the starting point for exploring the geometric and electronic structure of flavin ions in radical and reduced states using the IRMPD technique.

2. Results and Discussion

Below, we compare the experimental IRMPD spectra with our DFT results. The heterocyclic ring system contains basic centers in the pyrazine (II) and pyrimidinedione (III) rings and the flavins can be protonated at these positions depending on the corresponding proton affinities. In order to discuss the effect of protonation on the structure of the flavins, we calculated the energies, structures, and corresponding harmonic vibrational frequencies of the neutral and possible prototropic isomers. We abbreviate the neutral flavin as FI and the corresponding protonated form as H⁺FI where FI=LC, LF, RF, and FMN. A specific isomer is denoted in the form H⁺FI@XY, where X refers to the protonated element (N or O) and Y to the position of X according to the numbering given in Figure 1c. In case of O-protonated forms, the notation + or – indicates the orientation of the H atom with respect to N3–H. When the H atom points away from N3–H, it is assigned as OY+, whereas the opposite configuration will be denoted as OY–. Flavins can principally undergo lactam–lactim tautomerism. The lactim tautomer is characterized by the migration of the proton at N3 to one of the C=O groups. Protonation of the lactim can then lead to the formation of two OH functional groups. In this case, we use the notation H⁺FI@OH. The signs + or – denote the orientation of the O2–H (first sign) and O4–H (second

sign) following the same rule as described above. In practice, the +– conformation depicts a counterclockwise orientation of the H atoms, while in ++ both H atoms point to the far side of N3.

The reported energies of individual isomers are relative Gibbs free energies at 298 K, G_{rel} . The energetically lowest-lying isomer found in our calculations is set at $G_{\text{rel}}=0$. Carbon-protonated species are not included in this analysis because of their expected high G_{rel} .^[62,63] This assumption is supported by our exemplary calculation of H⁺LF@C9, which yielded $G_{\text{rel}}=163 \text{ kJ mol}^{-1}$.

The presence of methyl groups attached to the chromophore can lead to the existence of energetically low-lying conformers separated by low rotational barriers. In our structural search we considered the presence of conformers caused by the rotation of the methyl group around the C8–CH₃ axis with respect to the C7 methyl group. Using LF as a reference molecule, the energies have been calculated by a 120° rotational scan of the C8 methyl group. The analysis revealed that the eclipsed conformation of both methyl groups is energetically favored by 56 kJ mol^{-1} . Furthermore, vibrational analysis of the staggered conformer yielded one imaginary frequency for the torsional vibration of the C8 methyl group. This result indicates that the conformer with staggered orientation represents a transition state. Therefore, for all other compounds and their isomers, we considered only the eclipsed conformation without further verification. We also verified the existence of conformers in LF caused by methyl group rotation about the N10–C_α bond. Here, the staggered conformations with respect to the C8 methyl group are energetically favored and separated by a rotational barrier of 60 kJ mol^{-1} .

In the cases of RF and FMN, the number of potential low-energy rotamers increases drastically due to internal rotations of single bonds within the ribityl and ribophosphate side chains. Therefore, an individual conformational search for the lowest lying protonation states of both molecules was performed. The energetically low-lying conformations are classified by the orientation of the ribityl methylene group (C_αH₂) directly linked to the chromophore and by the formation of intramolecular H-bonds to the pyrimidinedione moiety (or internal H-bonds within the side chain). According to the methylene orientation, two stable conformers can be found. In conformer 1, the two H atoms are above the molecular plane (and the ribityl residue is below), whereas in conformer 2, the methylene H atoms point to the opposite side. In both conformations, the remainder of the ribityl and ribophosphate residues can adopt different orientations by forming single or multiple H-bonds to the chromophore via C_β–OH, C_γ–OH, C_δ–OH, C_ε–OH, P=O, and P–OH groups. In our nomenclature, to distinguish different structures of the first class of conformers we use Greek letters to indicate which ribityl OH group forms an H-bond with the pyrimidinedione moiety. When P–OH or P=O of the phosphate is involved in H-bonding we designate this with P or PO, respectively.

Comparison of the IRMPD spectrum with the theoretical IR spectra must take into account that the theoretical spectrum is linear, whereas the experiment relies on multiple-photon pro-

cesses which might introduce deviations from linearity. As a consequence of variations in anharmonic coupling or shifting and the resulting differences in multiple-photon excitation efficiencies, the calculated relative intensities and frequencies of certain vibrational bands might occasionally deviate slightly from the IRMPD data.^[64]

2.1. Protonated Lumichrome

H^+LC with mass $m=243$ u dissociates by IR multiple-photon absorption into three daughter ions with $m=200$, 198 and 172 u, which correspond to the formal loss of OCNH , $\text{CO}+\text{NH}_3$ or $\text{HCN}+\text{H}_2\text{O}$, and $\text{OCNH}+\text{CO}$, respectively. The depletion spectrum of the H^+LC parent ion agrees well with the appearance spectra of all daughter ions, indicating parallel rather than sequential photodissociation into the individual fragments (Figure S1 in the Supporting Information). The resulting IRMPD spectrum (Figure 2a) is dominated by intense IR bands at 1810 (A), 1745 (B), 1520 (D) and 1370 cm^{-1} (F) and lower-intensity bands at 1610 (C), 1450 (E), 1320 (G), and 1260 cm^{-1} (H), whereas the weakest features are observed at 880 (J) and 740 cm^{-1} (K).

We calculated all prototropic isomers of H^+LC arising from protonation of the five most basic centers of the alloxazine ring including lactim tautomers. Up to an energy of

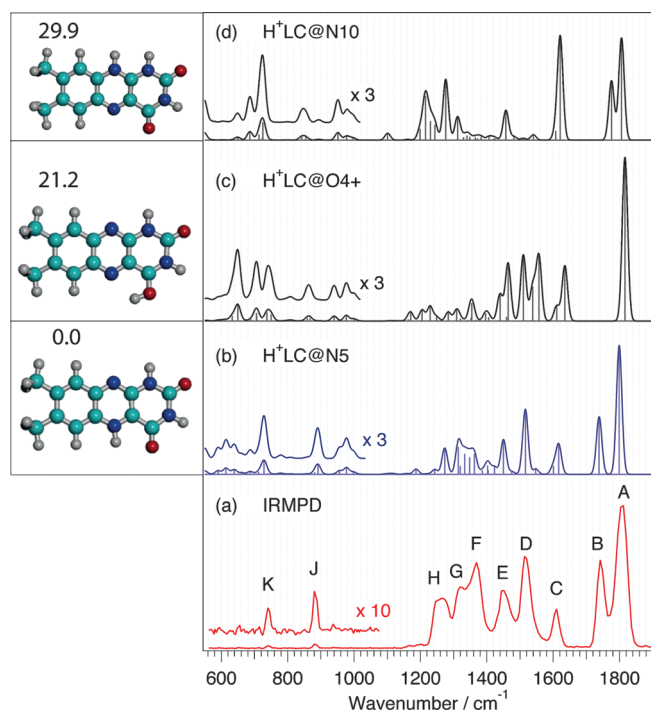


Figure 2. IRMPD spectrum of H^+LC (a) compared with linear IR spectra calculated at the B3LYP/cc-pVDZ level for the three most stable isomers— $\text{H}^+\text{LC@N5}$ (b), $\text{H}^+\text{LC@O4+}$ (c), and $\text{H}^+\text{LC@N10}$ (d). The theoretical stick spectra are scaled with 0.965 and convoluted with a 20 cm^{-1} FWHM contour. Peak positions in the IRMPD spectra (A–K) with their assignments are listed in Table S1. The spectra at lower frequencies are expanded by the indicated factors. The corresponding structures and relative Gibbs free energies [kJ mol^{-1}] are also shown.

72 kJ mol^{-1} we found seven different isomers (Figures 2 and S2). The most stable form (also denoted as ground state) is the N5-protonated species $\text{H}^+\text{LC@N5}$, followed by O4-protonated (also denoted as first excited state^[54]) $\text{H}^+\text{LC@O4+}$ ($G_{\text{rel}}=21.2\text{ kJ mol}^{-1}$) and the N10-protonated second excited state $\text{H}^+\text{LC@N10}$ ($G_{\text{rel}}=29.9\text{ kJ mol}^{-1}$). The latter can also be considered as N1-protonated iso-LC. The O-protonated isomers $\text{H}^+\text{LC@O4-}$, $\text{H}^+\text{LC@O2-}$, $\text{H}^+\text{LC@O2+}$, and its tautomer $\text{H}^+\text{LC@OH}++$ are energetically less favored, with $G_{\text{rel}}=58.9$, 68.8, 70.9, and 71.7 kJ mol^{-1} , respectively. The large stabilization of 37.7 kJ mol^{-1} for $\text{H}^+\text{LC@O4+}$ over the corresponding $\text{H}^+\text{LC@O4-}$ isomer can be explained by the additional interaction of the N5 lone pair with the additional proton at O4.

To identify the structure of the experimentally observed H^+LC isomer(s), the IRMPD spectrum was compared with the calculated linear IR spectra of the seven isomers considered (Figure S3). The IR spectra of the three most stable isomers are plotted in Figure 2 b–d above the experimental spectrum (Figure 2a). The spectrum calculated for the $\text{H}^+\text{LC@N5}$ ground-state isomer reproduces essentially all experimental vibrational features in terms of both the band positions and relative IR intensities. The spectrum calculated for the first excited isomer $\text{H}^+\text{LC@O4+}$ matches only the bands D, F, G and K of the IRMPD spectrum, whereas bands A and E are blueshifted, and band B is absent. In addition, intense bands at 1635, 1580, 705 and 620 cm^{-1} in the calculated spectrum are not observed in the experimental spectrum, strongly indicating that this isomer does not contribute to the IRMPD spectrum. The spectrum of the second excited $\text{H}^+\text{LC@N10}$ isomer shows agreement only for the experimental bands A, C and E, whereas D and F are absent and B appears at too high a frequency. Moreover, the vibrations near 1200 cm^{-1} are not present in the IRMPD spectrum. For the even less-stable isomers, the calculations also do not agree with experiment (Figure S3). Thus, contributions of isomers other than the most stable to the IRMPD spectrum are concluded to be minor.

According to the calculations, band A corresponds to the $\text{C}2=\text{O}$ stretch vibration $\nu_{\text{C}2=\text{O}}$ and B to $\nu_{\text{C}4=\text{O}}$ of $\text{H}^+\text{LC@N5}$. Both vibrations are largely decoupled and show significantly different IR intensities in which the $\text{C}2=\text{O}$ vibration is approximately twice as strong as the $\text{C}4=\text{O}$ mode. The experimental frequency splitting, $\nu_{\text{C}2=\text{O}}-\nu_{\text{C}4=\text{O}}=\Delta\nu_{\text{s,exp}}=65\text{ cm}^{-1}$, agrees well with the corresponding calculated value of $\Delta\nu_{\text{s,th}}=61\text{ cm}^{-1}$. Comparison of this value with the splitting predicted for $\text{H}^+\text{LC@N10}$, $\Delta\nu_{\text{s,th}}=30\text{ cm}^{-1}$, demonstrates the large influence of the protonation site on the $\text{C}4=\text{O}$ stretch frequency shift $\Delta\nu_{\text{C}4=\text{O}}$. A more detailed vibrational assignment of the observed bands (A–K) is given in Table S1.

2.2. Protonated Lumiflavin

The parent ion H^+LF ($m=257$ u) decomposes by IRMPD into five different fragment ions ($m=214$, 186, 171, 159, and 145 u). The fragment ion with $m=214$ u also shows strong depletion features, for example near 1580 and 1220 cm^{-1} , indicating sequential decay into the four remaining and competing fragment channels upon secondary IR absorption processes of this

primary fragment ion (Figure S4). The $m=214$ u channel corresponds to the formal loss of OCNH (or $\text{CO} + \text{CH}_3$), which is followed by further ring fragmentation arising from loss of CO ($m=186$ u), OCNH/ $\text{CO} + \text{CH}_3$ ($m=171$ u), $\text{CO} + \text{HCN}$ ($m=159$ u), and $\text{CO} + \text{CH}_3\text{CN}$ ($m=145$ u). The resulting IRMPD spectrum of H^+LF in Figure 3a differs significantly from that of H^+LC . The most intense vibrational bands are located at 1580 (C) and 1540 cm^{-1} (D), less intense vibrations at 1790 (B), 1490, 1340, 1230, and 1160 cm^{-1} (E–H), and weaker transitions at 1060 (J) and 840 cm^{-1} (K).

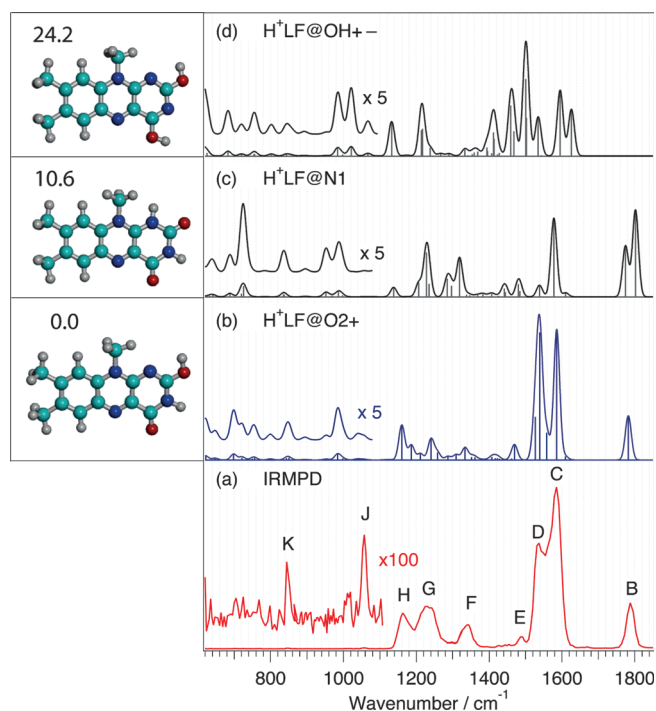


Figure 3. IRMPD spectrum of H^+LF (a) compared with linear IR spectra of the most stable isomers— $\text{H}^+\text{LF}@O_2+$ (b), $\text{H}^+\text{LF}@N_1$ (c), and $\text{H}^+\text{LF}@OH+-$ (d) calculated at the B3LYP/cc-pVDZ level of theory. The theoretical stick spectra are scaled with 0.965 and convoluted with a 20 cm^{-1} FWHM contour. Peak positions in the IRMPD spectra (B–K) with their assignments are listed in Table S2. The spectra at lower frequencies are expanded by the indicated factors. The corresponding structures and relative Gibbs free energies [kJ mol^{-1}] are also presented.

Guided by the H^+LC results, we have identified eight different H^+LF isomers up to an energy of 65 kJ mol^{-1} (Figures 3 and S5). Methylation of the N10 position changes the energetic order for the H^+LF isomers with respect to those of H^+LC . In agreement with Meyer et al.,^[52] our calculations predict the O_2 -protonated tautomer $\text{H}^+\text{LF}@O_2+$ to be the most stable isomer in the gas phase followed by the N_1 -protonated isomer $\text{H}^+\text{LF}@N_1$ with $G_{\text{rel}}=10.6$ kJ mol^{-1} . This energy difference agrees reasonably well with the value of 14 kJ mol^{-1} obtained by semi-empirical and ab initio methods by Meyer et al.^[52] Indeed, their single-point MP2 calculations showed that the energy gap between both tautomers significantly decreases, but the energetic order is preserved. However, protonation at

N_1 is experimentally observed in acidic solution,^[49] and the crystal structure analysis of 10-methylisalloxazine hydrobromide dihydrate reveals a proton bound to N_1 .^[14] These experimental results are supported by the SCRF calculations based on the Onsager model proposed by Meyer et al.^[52] To mimic the effect of water on the stability of the O_2 - and N_1 -protonated tautomers, the authors applied a polar medium with a relative permittivity $\epsilon=80$. Under these conditions, the N_1 proton becomes considerably more stabilized than the O_2 proton, indicating that the preferred protonation site shifts from O_2 to N_1 in solution. At higher energy, we find the tautomer $\text{H}^+\text{LF}@OH+-$, the second O_2 -protonated isomer $\text{H}^+\text{LF}@O_2-$, the next tautomer $\text{H}^+\text{LF}@OH++$, and $\text{H}^+\text{LF}@O_4+$, with $G_{\text{rel}}=24.2, 25.1, 29.7,$ and 34.4 kJ mol^{-1} , respectively. In contrast to H^+LC , the N_5 -protonated species $\text{H}^+\text{LF}@N_5$ is relatively unstable with $G_{\text{rel}}=48.6$ kJ mol^{-1} .

Previously, several authors have considered only the protonation of N_1 and N_5 . Our calculation yields an energetic difference of 38 kJ mol^{-1} between both isomers, which is about half Zheng's value^[13] but close to the value of 42 kJ mol^{-1} calculated at the B3LYP/TZVP level by Salzmann and Marian.^[65] They explain the preferred N_1 -protonation with the π -electron density in the doubly occupied π_{H} molecular orbital, which exhibits high electron density at N_1 and a node at N_5 . The second O_4 -protonated isomer $\text{H}^+\text{LF}@O_4-$ is found at $G_{\text{rel}}=64.2$ kJ mol^{-1} .

Figure 3 shows a comparison of the IRMPD spectrum to the calculated IR spectra of the three most stable H^+LF isomers, namely $\text{H}^+\text{LF}@O_2+$, $\text{H}^+\text{LF}@N_1$, and $\text{H}^+\text{LF}@OH+-$. Clearly, only the spectrum for the ground-state $\text{H}^+\text{LF}@O_2+$ (Figure 3b) agrees well with the experimental spectrum. All vibrational band positions in the IRMPD spectrum are reproduced by the calculation (see Table S2 for a detailed assignment). The strongest evidence for the presence of $\text{H}^+\text{LF}@O_2+$ is the observation of only one of the initial two $\nu_{\text{C}=\text{O}}$ vibrations. The low intensity indicates that this band is correlated with $\nu_{\text{C}4=\text{O}}$ which is labeled B. The formation of the OH group upon O_2 protonation leads to a drastic IR absorption enhancement of the ring N_1 – C_2 (C) and N_1 – C_{10a} stretch vibrations (D), both of which are coupled with the angular deformation of the C_2 – O – H bond. These characteristic vibrational features are only reproduced by the O_2+ tautomer. There is no obvious evidence for the coexistence of the energetically close-lying $\text{H}^+\text{LF}@N_1$ isomer. Weak arguments for the minor presence of $\text{H}^+\text{LF}@N_1$ include the relative intensities of the bands C and D and the relatively high intensity of band G, which are not perfectly reproduced by the spectrum calculated for $\text{H}^+\text{LF}@O_2+$. However, the clear absence of the strongest $\text{H}^+\text{LF}@N_1$ absorption arising from its $\nu_{\text{C}2=\text{O}}$ mode at 1801 cm^{-1} in the experimental spectrum provides a strong argument against any abundance of $\text{H}^+\text{LF}@N_1$. Similarly, the second tautomer $\text{H}^+\text{LF}@OH+-$ can be directly excluded because its calculated spectrum is completely different from the experimental one. The same conclusion holds for the other five isomers that are higher in energy (Figure S6).

2.3. Protonated Riboflavin

The H^+RF parent ion ($m=377$ u) undergoes IRMPD into three fragment ions with $m=243$, 198 and 172 u (Figure S7). The dominant dissociation channel arises from the loss of the ribityl moiety, which leads to the formation of H^+LC ($m=243$ u) with approx. 30% of the total parent depletion signal. The other two channels ($m=198$ and 172 u) are comparatively weak, and their action spectra differ from the main $m=243$ u channel. Moreover, the same two fragmentation channels have also been observed upon IRMPD of bare H^+LC identified as $\text{H}^+\text{LC}@N5$. Except for the $\text{C}=\text{O}$ stretch region around 1780 cm^{-1} and a comparatively too strong signal at 1160 cm^{-1} we find reasonable agreement of the signal positions in the fragment spectra of $m=198$ and 172 u from bare H^+LC and H^+RF (Figure S8). This observation strongly indicates that the primary

H^+LC product formed upon IRMPD of H^+RF dissociates by secondary IR absorption into the smaller fragment ions. Moreover, this assumption is clearly supported by the fact that the vibrational band near 1050 cm^{-1} (I)—related to the excitation of the $\text{C}_\beta\text{--C}_\gamma$ stretch and $\text{C}_\gamma\text{--O--H}$ deformation of the ribityl unit observed in the H^+LC channel ($m=243$ u)—is absent in the spectra of the secondary 198/172 u fragment ions.

The IRMPD spectrum of H^+RF in Figure 4a shows the most intense transitions around 1795 (A), 1770 (B), and 1600 cm^{-1} (C). Strong absorptions are also observed around 1330, 1260, 1220, and 1160 cm^{-1} (E–H), whereas much weaker bands appear around 1500 (D), 1050, 850, and 750 cm^{-1} (I–K).

Guided by the H^+LF results and HF calculations, we performed calculations for H^+RF isomers with protonation at N1 and O2, with different low-energy ribityl conformations. For N1 protonation, we found four conformers of class 1 and three of class 2 below 32 kJ mol^{-1} . Their different chain conformations allow for the formation of H-bonds between different ribityl hydroxyl groups and the N1 proton (Figure S9). The lengths of the H-bonds for the individual low-energy conformers are given in Table S3. In the ground-state $\text{H}^+\text{RF-1}\beta@N1$ isomer, the intramolecular $\text{NH}\cdots\text{O}$ H-bond is formed between N1--H and $\text{C}_\beta\text{--O(H)}$. The first excited conformer $\text{H}^+\text{RF-2}\gamma@N1$ at 7.0 kJ mol^{-1} is obtained by rotating the entire chain about the N10--C_α axis by 180° . In this case, the $\text{NH}\cdots\text{O}$ H-bond is formed between $\text{C}_\gamma\text{--O(H)}$ and the N1--H proton. The corresponding conformer 1, $\text{H}^+\text{RF-1}\gamma@N1$, lies 5.8 kJ mol^{-1} higher in energy than conformer 2. This difference can be explained by less efficient intramolecular interactions between hydroxyl groups within the ribityl residue for the $\text{H}^+\text{RF-2}\gamma@N1$ conformation. The second and third excited H^+RF isomers, $\text{H}^+\text{RF-2(1)}\delta@N1$, are the N1-protonated conformers 2 and 1 with an $\text{NH}\cdots\text{O}$ H-bond between N1--H and $\text{C}_\delta\text{--O(H)}$, which are energetically separated by only 0.1 kJ mol^{-1} . The fifth low-energy isomer, $\text{H}^+\text{RF-2}\varepsilon@N1$ at 17.3 kJ mol^{-1} , corresponds to conformer 2 stabilized by $\text{NH}\cdots\text{O}$ H-bonding between $\text{C}_\varepsilon\text{--O(H)}$ and N1--H . 14.4 kJ mol^{-1} higher in energy, we find the corresponding conformer 1, $\text{H}^+\text{RF-1}\varepsilon@N1$. The lowest-energy O2 tautomer, $\text{H}^+\text{RF-2}@O2$, lies 26.2 kJ mol^{-1} above the ground-state conformation and does not form an H-bond to the chromophore. Al-

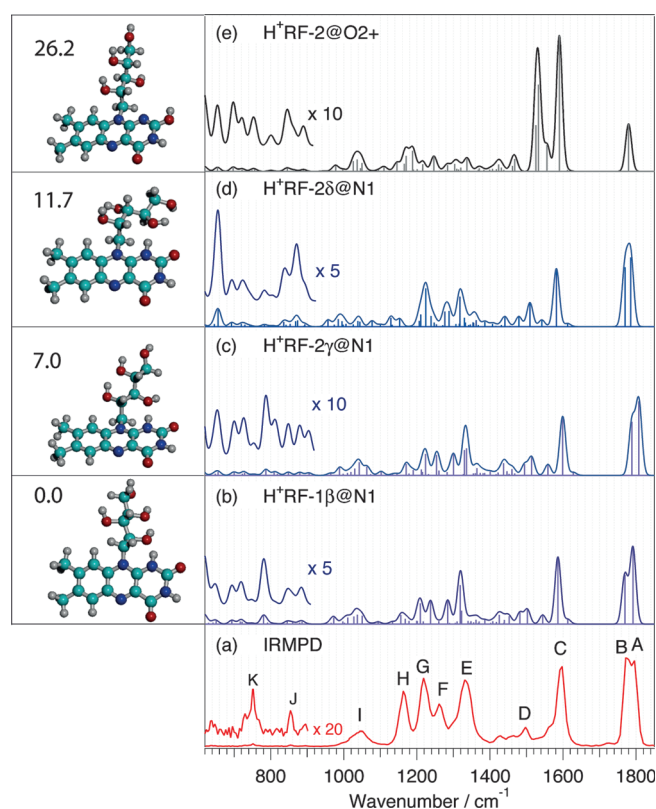


Figure 4. IRMPD spectrum of H^+RF (a) compared with theoretical linear IR spectrum of the most stable isomers— $\text{H}^+\text{RF-1}\beta@N1$ (b), the conformer $\text{H}^+\text{RF-2}\gamma@N1$ (c), $\text{H}^+\text{RF-2}\delta@N1$ (d), and $\text{H}^+\text{RF-2}@O2+$ (e). The theoretical stick spectra are scaled with 0.965 and convoluted with a 20 cm^{-1} FWHM contour. Peak positions in the IRMPD spectrum (A–K) with assignments are listed in Table S4. The spectra at lower frequencies are expanded by the indicated factors. The corresponding structures and relative Gibbs free energies [kJ mol^{-1}] are also presented.

though the majority of the N1-protonated isomers are close in energy, they are well separated by high internal rotation barriers on the order of 100 kJ mol^{-1} , arising from breaking intramolecular H-bonds. For example, the barrier between $\text{H}^+\text{RF-1}\beta@N1$ and $\text{H}^+\text{RF-2}\gamma@N1$ is calculated as 103 kJ mol^{-1} at the HF/6-31G level. Due to these large barriers, interconversion between these conformers in the gas phase at room temperature is not feasible. However, solvation might substantially affect their relative energies and isomerization barriers.

Figure 4 shows a comparison of the IRMPD spectrum of H^+RF (Figure 4a) to the spectra calculated for the three most stable N1-protonated isomers, $\text{H}^+\text{RF-1}\beta@N1$, $\text{H}^+\text{RF-2}\gamma@N1$ and $\text{H}^+\text{RF-2}\delta@N1$ (Figure 4b–d, respectively), as well as the most stable O2-protonated isomer, $\text{H}^+\text{RF-2}@O2+$ (Figure 4e). IR spectra of all low-energy H^+RF conformers considered are shown in Figure S10. Significantly, the IR spectra of the N1-protonated conformers are similar but clearly different from that of the O2-protonated isomer. In general, the calculated IR spectra of the N1-protonated conformers agree well with the IRMPD spectrum. In the experimental spectrum, two different $\text{C}=\text{O}$ stretch vibrations with almost the same high intensity appear around 1795 (A) and 1770 cm^{-1} (B), which immediately excludes an assignment to any (single) O2-protonated isomer.

The individual C=O frequencies (as well as further modes), intensity ratios and frequency splittings $\Delta\nu_{s,\text{th}}$ of the different N1-protonated conformers show subtle variations (Figures 4 and S10). Depending on the intramolecular bond between the side chain and the N1 proton, the C=O frequency ranges from 1751 in $\text{H}^+\text{RF-}2\epsilon\text{@N1}$ to 1783 cm^{-1} in $\text{H}^+\text{RF-}1\epsilon\text{@N1}$, $\Delta\nu_{s,\text{th}}$ lies between -10 and 26 cm^{-1} , and the C=O/C4=O intensity ratio changes from 1 to a maximum of 1.5. Unfortunately, the experimental resolution is insufficient to unambiguously distinguish between these spectral differences. Similar conclusions apply to the other parts of the recorded spectrum. Regarding the peak positions, the best agreement between calculation and experiment is obtained for the most stable and the first excited isomer. We therefore assume that both $\text{H}^+\text{RF-}1\beta\text{@N1}$ and $\text{H}^+\text{RF-}2\gamma\text{@N1}$ dominate the IRMPD spectrum with possible contributions from the higher-energy conformer. A list of peak positions of the IRMPD spectrum with vibrational assignments is available in Table S4.

2.4. Protonated Flavin Mononucleotide

H^+FMN ($m=457 \text{ u}$) is the most complex flavin molecule considered in this study. It shows a complex fragmentation pattern of the side chain upon IRMPD, while the aromatic chromophore does not decompose. We identified three main photo-products with $m=421$, 359, and 341 u, corresponding to the formal loss of two H_2O molecules, phosphoric acid (H_3PO_4), and $\text{H}_2\text{O} + \text{H}_3\text{PO}_4$, respectively. The loss of H_2O and H_3PO_4 was observed in a recent collision-induced dissociation study, whereas the fragmentation into H^+LC only occurred at an excitation wavelength of 435 nm through UVPD.^[53] This result supports the suggestion that the randomization of the introduced energy by collision or IR multiple-photon absorption and the dissociation dynamics of both processes in the ground electronic state are similar. Only at high photon flux, was the formation of H^+LC ($m=243 \text{ u}$), corresponding to the loss of the entire ribophosphate group $\text{CH}_2\text{-(CHOH)}_3\text{-OP=O(OH)}_2$, observed as an IRMPD process.

The IRMPD spectrum of H^+FMN recorded under low laser flux conditions (Figure 5a) shows intense vibrational features at 1780, 1590, 1540 (A–D), 1260 (F) and 1220 cm^{-1} (G), whereas slightly less-intense transitions were observed at 1340 (E), 1160, 1060, 1020, and 930 cm^{-1} (H–K).

Guided by the results of H^+LF and HF calculations, we considered only N1- and O2-protonated isomers. The phosphate group in the side chain of H^+FMN increases conformer flexibility and therefore the number of potential low-energy conformers. Indeed, according to our calculations (at least) 12 conformers exist up to an energy of 25 kJ mol^{-1} . Five conformers are protonated at N1, seven at O2, and only three belong to conformer class 1, whereas nine are part of class 2 (Figure S11). The calculation predicts the O2-protonated conformer $1\text{PO-}1\text{@O2}^+$ stabilized by three H-bonds in the ground state. In this case, the P=O group is the acceptor for two bifurcated H-bonds with the donors O2–H and $\text{C}_\gamma\text{O-H}$, and a third H-bond is formed by the OH groups at C_β and C_δ . Also, the next four excited conformers of H^+FMN are protonated at O2 and

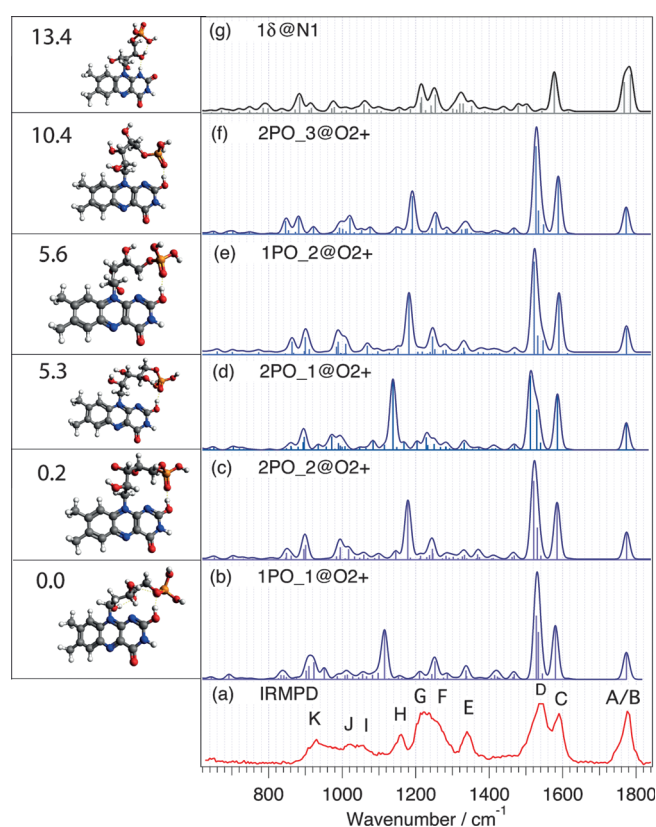


Figure 5. IRMPD spectrum of H^+FMN (a) compared with theoretical linear IR spectra of the low-energy conformers— $1\text{PO-}1\text{@O2}^+$ (b), $2\text{PO-}1\text{@O2}^+$ (c), $2\text{PO-}2\text{@O2}^+$ (d), $1\text{PO-}2\text{@O2}^+$ (e), $2\text{PO-}3\text{@O2}^+$ (f) and $1\delta\text{@N1}$ (g). The frequencies are scaled with 0.965 and the line spectrum convoluted with a 20 cm^{-1} FWHM contour. Peak positions in the IRMPD spectrum (A–K) with their assignments are listed in Table S6. The corresponding structures and relative Gibbs free energies [kJ mol^{-1}] are also presented.

H-bonds are formed between P=O and the O2–H proton. The first conformer in this series is $2\text{PO-}2\text{@O2}^+$, which belongs to class 2 and lies only 0.2 kJ mol^{-1} above the most stable isomer. In this isomer, the ribophosphate can adopt a conformation in which the P=O group is located in the molecular plane and interacts with the proton at O2. Such a small energy difference calculated at the B3LYP/cc-pVDZ level might not reflect the correct energetic order. More reliable results can be achieved by comparing the single-point energies calculated at the MP2 level.^[66] In fact, the MP2/cc-pVDZ calculation reverses the order for both H^+FMN isomers. According to that calculation, $2\text{PO-}2\text{@O2}^+$ is the ground-state conformer, stabilized by 2.1 kJ mol^{-1} with respect to $1\text{PO-}1\text{@O2}^+$.

The second excited isomer, $2\text{PO-}1\text{@O2}^+$, corresponds to conformer 2 of the ground-state isomer. The free energy difference between conformers 1 and 2 of 5.3 kJ mol^{-1} can be explained by the absence of the $\text{C}_\beta\text{OH}\cdots\text{OC}_\gamma$ H-bond which is not possible in conformer 2. Similar behavior is found by comparing conformers 2 and 1 of the first excited isomer. The higher excited conformation, $1\text{PO-}2\text{@O2}^+$, does not facilitate an effective interaction between the OH groups within the ribophosphate as in the lower-lying $2\text{PO-}2\text{@O2}^+$ isomer, although the $\text{PO}\cdots\text{HO2}$ bond becomes shorter. For this conformer pair,

almost the same energy difference is calculated (5.2 kJ mol^{-1}). The conformation 2PO-3@O2^+ is a variant in which the oxygen of the phosphate ester points to the chromophore and defines the $\text{P=O}\cdots\text{H}$ angle which is 140° . This conformer can be transformed in conformation 2PO-4@O2^+ via rotation around the $\text{C}_\gamma\text{-C}_\epsilon$ bond lifting the phosphate ester oxygen and locating the P=O group at a $\text{P=O}\cdots\text{H}$ angle close to 180° . In this conformation, the lone pairs of the phosphate oxygens approach each other more closely than in the 2PO-4@O2^+ conformer, leading to an energy increase.

The most stable N1-protonated isomer, $1\delta\text{@N1}$, lies 13.4 kJ mol^{-1} above the ground-state isomer. In this ion, the ribophosphate adopts a conformation in which the OH group at C_δ interacts with the N1 proton and one of the P-OH groups. The second N1-protonated conformer, $2\delta\text{@N1}$, lies 5.2 kJ mol^{-1} higher in energy compared to the first N1-protonated isomer. The conformation of the 2δ isomer facilitates the formation of the indicated $\text{C}_\delta\text{-O(H)}\cdots\text{HN1}$ bond and an additional $\text{C2=O}\cdots\text{HOP}$ bond. For the next higher lying N1-protonated isomers, see Figure S11. The corresponding H-bond lengths for the individual conformers are given in Table S5.

Figure 5 shows a comparison of the measured IRMPD spectrum with the calculated linear IR spectra and structures of the five most stable O2-protonated isomers and the most stable N1-protonated isomer identified for H^+FMN . The IRMPD spectrum satisfactorily agrees with the calculated IR spectra of all five O2-protonated, low-energy conformers in the high-frequency range of $1500\text{--}1850 \text{ cm}^{-1}$, with the exception of the clearly visible shoulder at 1750 cm^{-1} (A/B). As the C2=O stretch vibration is absent for all O2-protonated conformers and the C4=O stretch vibration appears at the same frequency (at 1770 cm^{-1}), this shoulder might directly indicate that not only O2-protonated conformers contribute to the IRMPD spectrum but also N1-protonated species.

The IRMPD spectrum reasonably agrees with the calculated IR spectrum of the ground-state conformer 1PO-1@O2^+ , except for the discrepancy of -40 cm^{-1} between the measured and calculated position of the band at 1160 cm^{-1} (H). This band corresponds to the P=O stretch mode which is sensitive to the conformation and the H-bonding, and might therefore be used as a fingerprint for the presence of a specific conformer. The first excited conformer 2PO-2@O2^+ , only 0.2 kJ mol^{-1} higher in free energy, shows the sharp P=O stretch band around 1175 cm^{-1} , i.e. slightly blueshifted with respect to the IRMPD feature H at 1160 cm^{-1} . Although the low-frequency signals appear slightly redshifted, the main peaks are in good agreement with the measured IRMPD spectrum. This observation might indicate that this conformer also contributes significantly to the IRMPD spectrum. The IR spectrum calculated for the second excited isomer, 2PO-1@O2^+ , also shows satisfactory agreement with the IRMPD spectrum but differs slightly from the other conformers. The band around 1500 cm^{-1} is broader and slightly redshifted. Thus, a minor contribution of this conformer to the IRMPD spectrum could explain the low-frequency shoulder of band D. The intense P=O mode at 1140 cm^{-1} is redshifted by -20 cm^{-1} with respect to the IRMPD band H and the vibrations between $800\text{--}900 \text{ cm}^{-1}$ are

shifted to lower frequency from those measured. The IR spectra of the third and fourth excited conformers, 1PO-2@O2^+ and 2PO-3@O2^+ , agree well with the IRMPD spectrum, except for the P=O stretch frequency which is slightly blueshifted from the experimental (band H). A similar redshift for the vibrations between $800\text{--}900 \text{ cm}^{-1}$ is also observed for this isomer. These shifts are of the same magnitude as for 2PO-2@O2^+ , because of the similar orientation of the P=O group with respect to O2-H . Making a clear distinction between the conformers from analysis of the frequency range $800\text{--}1100 \text{ cm}^{-1}$ is complicated because of the poorly resolved IRMPD spectrum. Although the profile of the calculated IR bands for the individual conformers show small variations, these features become unresolved when several conformers contribute to the IRMPD spectrum.

A discrepancy between the calculated P=O fingerprint mode of the H^+FMN conformers and the observed IRMPD bands might also arise from an unsuitable scaling factor. The scaling factor of 0.965 used here is a typical value that is applied for a large variety of organic molecules and fits the C=O stretch range well. Correia et al. and Rodgers and co-workers showed that the IR spectra agree well with the corresponding experimental IRMPD spectrum when the frequencies in the low-energy range arising from P-O and P=O stretch modes (below 1300 cm^{-1}) are unscaled.^[54,67] By applying a scaling factor of 1 to the P=O frequencies of the O2-protonated conformers of H^+FMN , the band of the ground-state conformer would blueshift to 1155 cm^{-1} , those of the first, third and fourth excited conformers to 1220 cm^{-1} , and that of the second excited conformer to 1175 cm^{-1} . Following this scenario, the ground-state P=O stretch would match the observed band H, the P=O stretch of the first excited state would fit the broad unresolved but intense band G, whereas the P=O stretch of the second excited conformer would coincide with neither H nor G. Taking this fact into consideration, the contribution of the 2PO-1@O2^+ conformer to the IRMPD spectrum can only be minor.

The IR spectrum calculated for the most stable N1-protonated isomer, $1\delta\text{@N1}$, is totally different from those of the O2-protonated isomers. However, it shows good agreement with the experimental spectrum in the C2=O and C4=O stretch region around 1750 cm^{-1} and in the range $1200\text{--}1300 \text{ cm}^{-1}$, matching the bands A/B and G, respectively. The isolated transition at 1580 cm^{-1} corresponds with band C (but is slightly redshifted), whereas the calculated band profile around 1320 cm^{-1} shows a somewhat stronger redshift compared to experiment (band E). The asymmetric shape of the IRMPD band A/B is also well reproduced by the calculation. This particular signature is not observed in the other spectra calculated for the low-energy O2-protonated conformers. Thus, although its free energy with respect to the ground-state O2-protonated isomer is relatively high (13.4 kJ mol^{-1}), contribution of the N1-protonated conformer to the IRMPD spectrum is suggested.

In summary, the calculations suggest contributions of (at least) the two most stable O2-protonated and the lowest energy N1-protonated isomers to the experimental IRMPD spectrum of H^+FMN .

2.5. Influence of Protonation on the Structure and Charge Distribution

In this section, we focus on the effects of protonation on the properties of the C=O bonds. The frequency shift of the C=O stretching modes of FMN in aqueous solution correlates with the strength of the H-bonds formed between the carbonyl groups and the protic solvent.^[19] The stronger the H-bond, the longer the C=O bond is, and the larger the frequency redshift. Similar to H-bonding, protonation can also have a significant impact on the structure of the flavin. Table 1 summarizes the

H⁺RF-2γ@N1. In contrast to LC and LF, both C=O bonds in RF-2γ contract by about $\Delta R_{C=O} = -1.1$ pm upon N1 protonation. Although $\Delta R_{C=O}$ is of the same magnitude, the resulting blueshifts for $\nu_{C=O}$ and $\nu_{C4=O}$ differ substantially (Figure S12e and f). The calculated $\Delta\nu_{C=O}$ shift is roughly two times larger than $\Delta\nu_{C4=O}$. Upon N1 protonation the H-bond shortens significantly. This leads to an elongation of the N1–C2 and C10a–N1 bonds as well as to a contraction of the C2=O bond, resulting in a $\nu_{C=O}$ blueshift. Small shift variations in H⁺RF-1β@N1 and H⁺RF-2γ@N1 reflect the subtle influence of the H-bond strength on the neighboring bond lengths. Due to the stronger H-bond in H⁺RF-2γ@N1, the N1–H, N1–C2 and C10a–N1 bonds are shorter, and consequently the C2=O bond is longer than in H⁺RF-1β@N1 (Table 1).

The planarity of the FMN chromophore is also preserved upon protonation at O2. The most stable neutral FMN-2P isomer possesses two unequal C=O bond lengths in contrast with the other flavin molecules considered. The C2=O bond is unusually long (123.5 pm) compared to those bonds of LC, LF, and RF-2γ, which scatter in a small range between 121.4–121.7 pm. This structural peculiarity is related to the presence

FI/H ⁺ FI	$R_{C=O}$ [pm]	$\nu_{C=O}$ [cm ⁻¹] ($\nu_{0,C=O}$ [cm ⁻¹])	$R_{C4=O}$ [pm]	$\nu_{C4=O}$ [cm ⁻¹] ($\nu_{0,C4=O}$ [cm ⁻¹])	PA [kJ mol ⁻¹]
LC	121.43	1766 (1830)	121.22	1748 (1811)	
H ⁺ LC@N5	120.22	1799 (1864)	121.61	1739 (1802)	935
LF	121.55	1731 (1794)	121.51	1743 (1806)	
H ⁺ LF@O2+	131.90	-	120.25	1782 (1847)	974
H ⁺ LF@N1	120.32	1802 (1867)	120.35	1775 (1839)	961
RF-1β	121.60	1730 (1793)	121.60	1739 (1802)	
H ⁺ RF-1β@N1	120.49	1791 (1856)	120.54	1770 (1834)	1007
RF-2γ	121.71	1726 (1789)	121.45	1743 (1806)	
H ⁺ RF-2γ@N1	120.66	1789 (1854)	120.51	1770 (1835)	997
FMN-2P	123.50	1663 (1723)	121.50	1748 (1811)	
H ⁺ FMN: 2PO-2@O2+	130.00		120.51	1774 (1838)	1011
2δ@N1	122.52	1730 (1793)	120.38	1778 (1842)	994

calculated C=O bond lengths, $R_{C=O}$ and $R_{C4=O}$, of the neutral molecules and their most stable protonated isomers, as well as the corresponding C=O stretch frequencies, $\nu_{C=O}$ and $\nu_{C4=O}$. Because the most stable neutral RF and FMN isomers are class 2 conformers, we consider here only the low-energy conformers H⁺RF-2γ@N1, H⁺FMN-2PO-2@O2+, and H⁺FMN-2δ@N1. The IR spectra of the neutral FI and corresponding H⁺FI are compared in Figure S12.

The addition of a proton to LC at N5 does not affect its planarity. The new N5–H bond induces an elongation of the neighboring C4a–N5 bond and a contraction of the C4–C4a bond by 1.5 and 1.3 pm, respectively. The C4=O bond is then slightly elongated by 0.4 pm leading to a modest C4=O stretch frequency redshift of $\Delta\nu_{C4=O} = -9$ cm⁻¹ (Figure S12a and b). In contrast, the C2=O bond contracts by more than 1.2 pm, significantly blueshifting the stretch frequency by $\Delta\nu_{C=O} = 33$ cm⁻¹ in the protonated form.

The LF skeleton also remains planar upon protonation of the C2=O group in H⁺LF@O2+. The C2=O bond drastically elongates by more than 10 pm, which reflects the loss of the C=O double bond character upon formation of a C–OH single bond. Therefore, the C2=O carbonyl stretch band is absent in the IR spectrum of H⁺LF@O2+ (Figures 3b and S12d). The C4=O bond contracts by more than 1.2 pm upon protonation, leading to a large frequency blueshift of $\Delta\nu_{C4=O} = 32$ cm⁻¹.

The approximate planarity of the isoalloxazine ring in neutral RF-2γ is conserved upon protonation at N1, leading to

of an intramolecular H-bond between the phosphate group and C2=O that is much shorter than that between ribityl and N1 as observed in RF-2γ. Upon O2 protonation the C2=O bond elongates by 6 pm but does not reach the value for H⁺LF@O2+. Again, formation of the O–H bond leads to the loss of the intense C2=O stretch vibration. The C4=O bond length is reduced by 1.1 pm resulting in a $\nu_{C4=O}$ blueshift of 26 cm⁻¹ (Figure S12g and h).

Upon N1 protonation, the C2=O bond in H⁺FMN-2δ undergoes a large blueshift of $\Delta\nu_{C=O} = 67$ cm⁻¹, reflecting the bond length reduction of 1.0 pm and a drastic H-bond elongation. A second, but much shorter H-bond is formed between the N1–H and O=P groups. The C4=O bond contracts by 1.1 pm, and its frequency increases, $\Delta\nu_{C4=O} = 30$ cm⁻¹. Compared to the other considered protonated flavins, upon protonation, the C2=O bond is significantly longer such that the more intense transition A appears at lower frequency than B.

To establish a correlation between the C=O bond lengths and their stretch frequencies, the calculated $\nu_{C=O}$ values are plotted as a function of $R_{C=O}$ in Figure 6 for the neutral flavins, the most stable and experimentally observed protonated H⁺FI, and the N1-protonated isomers H⁺FI@N1 (Table 1). Because of preferential O2 protonation in LF and FMN-2P, the corresponding cations have no C2=O carbonyl group. The data were fitted to a linear function of the form $\nu_{C=O}(R_{C=O}) = b_{C=O}R_{C=O} + a_{C=O}$, where the slope $b_{C=O}$ reflects the frequency shift in cm⁻¹ per 1 pm bond length change. The values in Table 1 show that

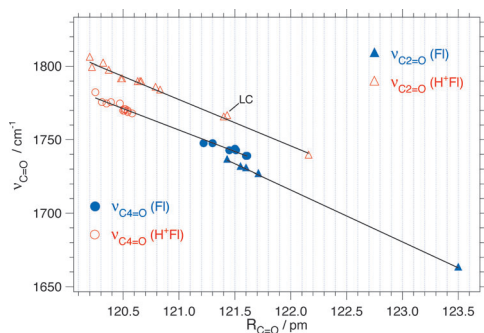


Figure 6. Correlation of the C=O stretch frequencies $\nu_{C=O}$ (triangle) and $\nu_{C4=O}$ (circle) with the C=O bond lengths $R_{C2=O}$ and $R_{C4=O}$ for six neutral (filled) and 13 protonated isomers of LC, LF, RF, and FMN (unfilled) including conformers. In neutral LC $\nu_{C2=O}$ is shifted to values typical for N1-protonated FI species. Values for the most stable and N1-protonated isomers are summarized in Table 1. For $H^+LF@O2+$ and $H^+FMN-2@O2+$, no $\nu_{C2=O}$ value is given. $\nu_{C=O}(R_{C=O})$ are fitted by the following functions:
 $\nu_{C2=O}(R_{C2=O}) = (-36 \pm 2)R_{C2=O} + (5641 \pm 272)$ for neutral and
 $\nu_{C2=O}(R_{C2=O}) = (-32 \pm 1)R_{C2=O} + (6081 \pm 127)$ for the protonated isomers, and
 $\nu_{C4=O}(R_{C4=O}) = (-30 \pm 1)R_{C4=O} + (5338 \pm 120)$ for neutral and protonated species.

$R_{C2=O}$ and $R_{C4=O}$ of iso-LC, LF, RF, and FMN are of almost equal length and contract upon N1 protonation by around 1 pm, respectively. In a first approximation, we therefore expect the $\nu_{C2=O}$, $\nu_{C4=O}$, and corresponding $\Delta\nu_{C=O}$ values to be of a similar magnitude. However, two well-separated $\nu_{C=O}$ values and an approximately twice as large blueshift for the C2=O mode compared to that for C4=O are not only found in RF but also in all other FI species considered here. Therefore, both modes are fitted separately. The fit of the $\nu_{C4=O}(R_{C4=O})$ function results in $b_{C4=O} = (-30 \pm 2) \text{ cm}^{-1} \text{ pm}^{-1}$ for both FI and H^+ FI. In contrast, the $\nu_{C2=O}(R_{C2=O})$ dependence shows a change in $b_{C2=O}$ from (-36 ± 2) to $(-32 \pm 2) \text{ cm}^{-1} \text{ pm}^{-1}$ and an abrupt strong rise in frequency when going from FI to H^+ FI. Furthermore, with the exception of LC, for a given $R_{C=O}$ the frequency splitting $\Delta\nu_{s,th}$ is of the order of 10 cm^{-1} in neutral flavins, i.e. the more intense C2=O vibration possesses a lower frequency than the less intense C4=O mode. Due to protonation, this $\Delta\nu_{s,th}$ value increases to around 25 cm^{-1} .

As $b_{C4=O}$ of FI is similar to that of H^+ FI, the $b_{C2=O}$ (and $a_{C2=O}$) deviation for neutral and protonated species indicates that the presence of the proton at N1 has an additional impact on the C2=O stretch vibration. Closer inspection reveals that both C=O stretching normal modes are not fully localized motions but involve couplings to bending vibrations of neighboring groups. In neutral flavins, the C4=O as well as the C2=O vibration mainly couples to the deformation motion of N3–H (indicated by the displacement vectors in Figure S13a and b). Upon N1 protonation, this vibrational coupling does not significantly change for the C4=O vibration (Figure S13c) so that the $\nu_{C4=O}-R_{C4=O}$ linear relationship of FI is preserved for H^+ FI. However, the C2=O stretch mode couples to both N3–H and N1–H deformation motions in the presence of the N1 proton (Figure S13c). This leads to a larger C2=O frequency blueshift and causes the jump in the $\nu_{C2=O}(R_{C2=O})$ function when going from the neutral to the protonated molecule (Figure 6).

In LC, the hydrogen substituent of N1 increases $R_{C10a-N1}$ and reduces R_{C2-N3} compared to iso-LC, LF, and RF-2 γ . Thus, these bond lengths are similar to that of the protonated species whereas $R_{C2=O}$ and R_{N1-C2} are of the same magnitude as in the neutral species. This gives rise to the $\nu_{C2=O}$ blueshift, for which the calculated value fits well to the $\nu_{C2=O}(R_{C2=O})$ dependence for the other H^+ FI species.

The proton affinity (PA) of a molecule represents a fundamental chemical property for evaluating acid–base reactions. It can be calculated from the energy difference between the most stable protonated and neutral isomer. As we are mainly interested in the trend of PA along the flavin series, we used the difference between the zero-point corrected total energies at 0 K, neglecting the translational energy of the proton as well as the temperature dependence of the enthalpies of the corresponding molecules and ions. The PAs of the flavins investigated are listed in Table 1 and tend to increase along the series $LC < LF < RF < FMN$ (934, 973, 1007, 1011 kJ mol^{-1} , respectively). Due to tautomerization of iso-LC, LF is frequently used as model system for theoretical considerations of flavins and flavoproteins.^[13,51,52,65,66] The calculation of PA for protonation of LF at O2 and N1 at the HF/6-31G* level by Meyer et al. gives higher values than our DFT calculation and a further increase of the PA results when a larger basis set (HF/6-31G**//HF/6-31G*) is used.^[52] The best agreement with our DFT values is found for the values calculated at the MP2/6-31G*//HF/6-31G* level, which are slightly lower than our results (962.6 kJ mol^{-1} at N1 and 970.6 kJ mol^{-1} at O2). Recently, Zhang et al. measured the PA of LF as $PA(LF) = (951.0 \pm 8.4) \text{ kJ mol}^{-1}$ by proton-transfer reactions and calculated the corresponding PA(LF) values for N1, O2, N5 and O4 protonation at the B3LYP/6-31G* level.^[68] The highest PA(LF) was found for position N1 with $PA(LF) = 965.5 \text{ kJ mol}^{-1}$, which is in good agreement with our calculated value for the same protonation site (961 kJ mol^{-1} , Table 1). However, the value calculated by Zhang et al. for O2 protonation of 946.8 kJ mol^{-1} agrees better with their experimental value. Our theoretical PA(LF) is significantly higher due to larger stabilization of the O2-protonated tautomer with respect to the N1 isomer and cannot be compared with Zhang's value.^[68] The highest protonation energies are found for RF and FMN which are close in energy. Upon protonation, FMN also tends to tautomerize in the gas phase, so RF is the only compound which thoroughly follows the predicted N1 protonation.

The natural bond orbital (NBO) calculations indicate that the increase of PA basically correlates with the increase of positive charge localized at the extra proton, which is distributed over the side chain and the chromophore, but the intrinsic relation is not obvious. The charge differences upon N1 protonation of the FI molecules reveals that with increasing size of the substituent R the positive charge i) slightly increases at the excess proton, ii) strongly increases at R, and iii) decreases to a similar degree in the chromophore (Figure S14). Along the same series, the PA is the largest for RF and FMN.

3. Conclusions

The gas-phase IRMPD spectra of protonated LC, LF, RF (vitamin B₂), and the cofactor FMN have been measured in the fingerprint region. DFT calculations were used to identify the preferred protonation site, and determine the geometry, energy and vibrational structure of each individual flavin. For LC and LF, isomers with N1, N3, N5, O2, and O4 protonation, including all possible tautomers, have been systematically investigated. For RF and FMN only a limited selection of N1- and O2-protonated species were considered.

The most stable H⁺LC is the N5-protonated isomer, whereas the most stable H⁺LF is the O2-protonated isomer (or the tautomer of the N1-protonated species). Calculated IR spectra for both H⁺LC and H⁺LF are in good agreement with the respective experimental spectra. In H⁺LC@N5, the experimental frequency splitting $\nu_{\text{C}=\text{O}} - \nu_{\text{C}=\text{O}}$ and the C2=O/C4=O intensity ratio are well reproduced by the calculation. In H⁺LF@O2, the absence of the C2=O mode, the frequency and intensity of the C4=O mode, as well as the strong enhancement of the ring stretch vibration can be clearly identified. For H⁺RF we found the N1-protonated isomer in two conformations as the most stable species, for which the calculated IR spectra agree fairly well with the IRMPD spectrum. The shape and the intensity of the unresolved IRMPD band in the C=O stretch region supports the conclusion of N1 protonation, but the distinct assignment to individual conformers is not possible at the spectral resolution obtained in these experiments. For H⁺FMN we identified the O2-protonated isomer (tautomer of N1-protonated species) as the most stable form, and close in energy to the corresponding N1-protonated isomer, both of which are stabilized by intramolecular H-bonds to the phosphate group. The IRMPD spectrum does not perfectly agree with the calculation, but the peak shape within the C=O stretch region combined with the high-intensity gain of the ring mode supports the presence of two species, namely N1- and O2-protonated isomers. In addition, the analysis of the P=O stretch vibration of different O2 conformers excludes the significant contribution of conformer 2PO-1.

From theoretical studies of neutral flavins and the variety of protonated isomers we can conclude that their C2=O and C4=O stretch frequencies and their shifts can serve as sensitive markers for electronic changes at the chromophore and the H-bonding environment. The C2=O and the C4=O frequencies contain information about the protonation state of the flavin. In the neutral state, these stretch frequencies are usually found within the range 1720–1750 cm⁻¹, where the more intense C2=O mode appears at lower frequency. In the N1-protonated state both frequencies are blueshifted to the range 1760–1810 cm⁻¹, but the C2=O mode appears at higher frequency than the C4=O stretch vibration (without involvement of H-bonds). In the case of N5 protonation, the C4=O frequency remains close to the frequency for neutral flavin, around 1760 cm⁻¹. In H⁺LC@N5, the combination of the C2=O blueshift caused by N1 protonation and an unaffected C4=O stretch frequency caused by N5 protonation is observed. Protonation at O2 generally leads to a C4=O blueshift of approx. 40 cm⁻¹.

Experimental Section

Experiment

The IRMPD spectra of protonated LC, LF, RF, and FMN were recorded in the fingerprint range (600–1850 cm⁻¹) in a Fourier-transform ion cyclotron resonance mass spectrometer (FT-ICR-MS) equipped with an electrospray ionization (ESI) source and coupled to the IR beamline of the free-electron laser for infrared experiments (FELIX).^[69,70] LC, LF, RF, and FMN·Na⁺·2H₂O salt with reagent grades of 99, 97, 95, and 97%, respectively, were purchased from Sigma–Aldrich and used without further purification. The protonated species were produced by spraying a 0.2–2 mM solution of LC, LF, RF, and FMN·Na⁺ in a methanol/water/formic acid mixture (78:20:2; for FMN·Na⁺ 78:18:4) at a flow rate of approximately 10 μL min⁻¹.

After accumulation in a hexapole ion trap for 4 s, the ESI-generated ions were transferred into the ICR trap through an octopole ion guide. All the ions considered here are singly charged species. Subsequently, the ions were mass-selected in the ion trap and irradiated for 2 s with 20 macropulses from FELIX operating at a repetition rate of 10 Hz. The bandwidth of the FELIX radiation is ≈0.5% of the central wavelength (full width at half maximum, FWHM), which corresponds to 5 cm⁻¹ at 1000 cm⁻¹. However, the experimental resolution is much broader due to unresolved rotational structures and heating of the molecules during multiple-photon absorption processes.^[71] Calibration of the laser wavelength was achieved using a grating spectrometer with an accuracy of ±2 and ±6 cm⁻¹ at frequencies of 500 and 2000 cm⁻¹, respectively. Depending on the laser frequency, the step size varied between 3 and 8 cm⁻¹. Parent and fragment ion intensities, I_p and I_f , were monitored as a function of the laser frequency, and the IRMPD yield I_{IRMPD} was calculated using Equation (1):

$$I_{\text{IRMPD}} = \sum I_f / (I_p + \sum I_f) \quad (1)$$

The IRMPD yield was linearly normalized according to the IR laser power.

Computational Methods

DFT calculations at the B3LYP level of theory using the cc-pVDZ basis set were performed for the protonated flavins in order to identify various energetically low-lying isomers on the potential energy surface and to evaluate their structure, energetics, and IR spectral properties.^[72] Relative Gibbs free energies at 298 K were determined and included thermal corrections. Harmonic frequency analysis ensured the nature of minima (local or global) on the potential energy surface. The harmonic vibrational frequencies were scaled by the factor 0.965. The theoretical linear IR stick spectra were convoluted with a Gaussian width (FWHM) of 20 cm⁻¹ to facilitate convenient comparison with the experimental IRMPD spectra.

To identify the energetically favored protonation sites for RF and FMN, possible prototropic isomers in a fixed conformation were calculated at the HF/6-311G level. The lowest-energy isomers were selected and a systematic conformational search was then applied to find potential low-energy conformers. The energy of all conformers obtained by rotation around single bonds was optimized using the Merck molecular force field 94 (MMFF94) and the universal force field (UFF) implemented in the Avogadro software.^[73] Subsequently, structures identified within 30 kJ mol⁻¹ of the most stable isomer were optimized and their vibrational frequencies were calculated at the B3LYP/cc-pVDZ level using Gaussian 03.^[72]

We are aware that the B3LYP functional can result in increased errors of the calculated energies, in particular in larger molecules.^[66,74] To evaluate our most stable structure obtained by DFT, we also performed single-point MP2 calculations in case that the energy difference between the most stable and first higher-lying isomer becomes small ($< 5 \text{ kJ mol}^{-1}$). In any case, the identification of isomers is mostly based on their experimental IR fingerprint and not on their predicted relative or absolute energies.

Acknowledgements

This work was supported by Technische Universität Berlin and Deutsche Forschungsgemeinschaft (DO 729/6). The research leading to these results was funded by the European Community's Seventh Framework Programme (FP7/2007-2013) under grant agreement n. 226716. This work is part of the research program of FOM, which is financially supported by the Nederlandse Organisatie voor Wetenschappelijk Onderzoek (NWO). We gratefully acknowledge the excellent assistance by the FELIX staff (Britta Redlich et al.).

Keywords: DFT calculations · flavins · IR spectroscopy · protonation · structure elucidation

- [1] *Harper's Biochemistry, International Series* (Eds.: R. K. Murray, D. K. Granner, P. A. Mayes, V. W. Rodwell), 25th ed., McGraw-Hill, New York, 2000.
- [2] *Flavins and Flavoproteins: Proceedings of the Seventh International Symposium* (Eds.: V. Massey, H. Williams), Elsevier, New York, 1982.
- [3] *Comprehensive Series in Photochemical and Photobiological Science, Vol. 6* (Eds.: E. Silva, A. Edwards), RSC, Cambridge, 2006.
- [4] T. E. Swartz, T. S. Tseng, M. A. Frederickson, G. Paris, D. J. Comerci, G. Rajashekara, J. G. Kim, M. B. Mudgett, G. A. Splitter, U. A. Ugalde, F. A. Goldbaum, W. R. Briggs, R. A. Bogomolni, *Science* 2007, 317, 1090.
- [5] T. E. Swartz, S. B. Corchnoy, J. M. Christie, J. W. Lewis, I. Szundi, W. R. Briggs, R. A. Bogomolni, *J. Biol. Chem.* 2001, 276, 36493.
- [6] T. Kottke, J. Heberle, D. Hehn, B. Dick, P. Hegemann, *Biophys. J.* 2003, 84, 1192.
- [7] A. Losi, W. Gärtner, *Photochem. Photobiol.* 2011, 87, 491.
- [8] A. Losi, *Photochem. Photobiol.* 2007, 83, 1283.
- [9] A. Mattevi, *Trends Biochem. Sci.* 2006, 31, 276.
- [10] P.-S. Song, M. Sun, A. Koziolowa, J. Koziol, *J. Am. Chem. Soc.* 1974, 96, 4319.
- [11] J. D. Choi, R. D. Fugate, P.-S. Song, *J. Am. Chem. Soc.* 1980, 102, 5293.
- [12] S. Salzmann, C. M. Marian, *Photochem. Photobiol. Sci.* 2009, 8, 1655.
- [13] Y.-J. Zheng, R. L. Ornstein, *J. Am. Chem. Soc.* 1996, 118, 9402.
- [14] B. L. Trus, C. J. Fritchie, *Acta Crystallogr. Sect. B* 1969, 25, 1911.
- [15] M. Wang, C. J. Fritchie, *Acta Crystallogr. Sect. B* 1973, 29, 2040.
- [16] M. C. Kuo, J. B. R. Dunn, C. J. Fritchie, *Acta Crystallogr. Sect. B* 1974, 30, 1766.
- [17] C. J. Fritchie, R. M. Johnston, *Acta Crystallogr. Sect. B* 1975, 31, 454.
- [18] P. E. Werner, O. Ronnquist, *Acta Chem. Scand.* 1970, 24, 997.
- [19] I. Hazeckawa, Y. Nishina, K. Sato, M. Shichiri, R. Miura, K. Shiga, *J. Biochem.* 1997, 121, 1147.
- [20] J. Rodriguez-Otero, E. Martinez-Nunez, A. Pena-Gallego, S. A. Vazquez, *J. Org. Chem.* 2002, 67, 6347.
- [21] M. A. North, S. Bhattcharyya, D. G. Truhlar, *J. Phys. Chem. B* 2010, 114, 14907.
- [22] C. T. W. Moonen, J. Vervoort, F. Müller, *Biochemistry* 1984, 23, 4859.
- [23] R. M. Kowalczyk, R. Bittl, S. Weber, *J. Am. Chem. Soc.* 2004, 126, 11393.
- [24] J. Roslund, M. Roth, L. Guyon, V. Boutou, F. Courvoisier, J.-P. Wolf, H. Rabitz, *J. Chem. Phys.* 2011, 134, 034511.
- [25] E. Sikorska, I. V. Khmelinskii, D. R. Worrall, J. Koput, M. Sikorski, *J. Fluoresc.* 2004, 14, 57.
- [26] E. Sikorska, I. V. Khmelinskii, J. Koput, J.-L. Bourdelande, M. Sikorski, *J. Mol. Struct.* 2004, 697, 205.
- [27] E. Sikorska, I. V. Khmelinskii, W. Prukala, S. L. Williams, M. Patel, D. R. Worrall, J.-L. Bourdelande, J. Koput, M. Sikorski, *J. Phys. Chem. A* 2004, 108, 1501.
- [28] R. J. Stanley, H. Jang, *J. Phys. Chem. A* 1999, 103, 8976.
- [29] M. Kondo, J. Nappa, K. L. Ronayne, A. L. Stelling, P. J. Tonge, S. R. Meech, *J. Phys. Chem. B* 2006, 110, 20107.
- [30] M. M. N. Wolf, Ch. Schumann, R. Gross, T. Domratheva, R. Diller, *J. Phys. Chem. B* 2008, 112, 13424.
- [31] A. Haigney, A. Lukacs, R.-K. Zhao, A. L. Stelling, R. Brust, R.-R. Kim, M. Kondo, I. Clark, M. Towrie, G. M. Greetham, B. Illarionov, A. Bacher, W. Römisch-Margl, M. Fischer, S. R. Meech, P. J. Tonge, *Biochemistry* 2011, 50, 1321.
- [32] W. D. Bowman, T. G. Spiro, *Biochemistry* 1981, 20, 3313.
- [33] A. Weigel, A. Dobryakov, B. Klaumünzer, M. Sajadi, P. Saalfrank, N. P. Ernsting, *J. Phys. Chem. B* 2011, 115, 3656.
- [34] M. Takahashi, Y. Ishikawa, J.-i. Nishizawa, H. Ito, *Chem. Phys. Lett.* 2005, 401, 475.
- [35] J.-Y. Hasegawa, S. Bureekaew, H. Nakatsuji, *J. Photochem. Photobiol. A* 2007, 189, 205.
- [36] E. Breinlinger, A. Niemz, V. M. J. Rotello, *J. Am. Chem. Soc.* 1995, 117, 5379.
- [37] E. Breinlinger, V. M. J. Rotello, *J. Am. Chem. Soc.* 1997, 119, 1165.
- [38] J. J. Hasford, W. Kemnitzer, C. J. Rizzo, *J. Org. Chem.* 1997, 62, 5244.
- [39] G. Horváth, J. Illényi, L. Pusztay, K. Simon, *Acta Chim. Hung.* 1987, 124, 819.
- [40] R. Thijs, T. Zeegers-Huyskens, *Spectrochim. Acta Part A* 1984, 40, 307.
- [41] P. J. Tonge, P. R. Carey, *Biochemistry* 1992, 31, 9122.
- [42] P. J. Tonge, R. Fausto, P. R. Carey, *J. Mol. Struct.* 1996, 379, 135.
- [43] S. Ghisla, C. Thorpe, V. Massey, *Biochemistry* 1984, 23, 3154.
- [44] M. Kim, P. C. Carey, *J. Am. Chem. Soc.* 1993, 115, 7015.
- [45] S. Miertus, E. Scrocco, J. Tomasi, *Chem. Phys.* 1981, 55, 177.
- [46] A. Klamt, G. Schürmann, *J. Chem. Soc. Perkin Trans. 2* 1993, 799.
- [47] B. Rieff, G. Mathias, S. Bauer, P. Travan, *Photochem. Photobiol.* 2011, 87, 511.
- [48] H. F. Heelis, *Chem. Soc. Rev.* 1982, 11, 15.
- [49] K. H. Dudley, A. Ehrenberg, P. Hemmerich, F. Müller, *Helv. Chim. Acta* 1964, 47, 1354.
- [50] P. Zirak, A. Penzkofer, T. Mathes, P. Hegemann, *Chem. Phys.* 2009, 358, 111.
- [51] J. Wouters, F. Durant, B. Champagne, J.-M. Andre, *Int. J. Quantum Chem.* 1997, 64, 721.
- [52] M. Meyer, H. Hartwig, D. Schomburg, *J. Mol. Struct. THEOCHEM* 1996, 364, 139.
- [53] L. Guyon, T. Tabarin, B. Thuillier, R. Antoine, M. Broyer, V. Boutou, P.-J. Wolf, P. Dugourd, *J. Chem. Phys.* 2008, 128, 075103.
- [54] Y.-w. Nei, N. Hallowita, J. D. Steill, J. Oomens, M. T. Rodgers, *J. Phys. Chem. A* 2013, 117, 1319.
- [55] K. T. Crampton, A. I. Rathur, Y.-w. Nei, G. Berden, J. Oomens, M. T. Rodgers, *J. Am. Soc. Mass Spectrom.* 2012, 23, 1469.
- [56] M. Citir, C. S. Hinton, J. Oomens, J. D. Steill, P. B. Armentrout, *Int. J. Mass Spectrom.* 2012, 330–332, 6.
- [57] Y.-w. Nei, T. E. Akinyemi, C. M. Kaczan, J. D. Steill, G. Berden, J. Oomens, M. T. Rodgers, *Int. J. Mass Spectrom.* 2011, 308, 191.
- [58] a) M. Seydou, G. Grégoire, J. Liquier, J. Lemaire, J. P. Schermann, C. Desfrancois, *J. Am. Chem. Soc.* 2008, 130, 4187; b) L. MacAleese, P. Maître, *Mass Spectrom. Rev.* 2007, 26, 583; c) B. Lucas, G. Grégoire, J. Lemaire, P. Maître, F. Glotin, J. P. Schermann, C. Desfrancois, *Int. J. Mass Spectrom.* 2005, 243, 105; d) G. Grégoire, M. P. Gaigeot, D. C. Marinica, J. Lemaire, J. P. Schermann, C. Desfrancois, *Phys. Chem. Chem. Phys.* 2007, 9, 3082.
- [59] a) P. B. Armentrout, M. T. Rodgers, J. Oomens, J. D. Steill, *J. Phys. Chem. A* 2008, 112, 2248; b) P. B. Armentrout, M. T. Rodgers, J. Oomens, J. D. Steill, *J. Phys. Chem. A* 2008, 112, 2258; c) A. V. Heaton, N. Bowman, J. Oomens, J. D. Steill, P. B. Armentrout, *J. Phys. Chem. A* 2009, 113, 5519; d) C. R. Carl, T. E. Cooper, J. Oomens, J. D. Steill, P. B. Armentrout, *Phys. Chem. Chem. Phys.* 2010, 12, 3384.
- [60] a) R. Wu, T. B. McMahon, *J. Am. Chem. Soc.* 2007, 129, 11312; b) R. Wu, T. B. McMahon, *ChemPhysChem* 2008, 9, 2826; c) R. Wu, T. B. McMahon, *J. Phys. Chem. B* 2009, 113, 8767.
- [61] a) A. Lagutschenkov, J. Langer, G. Berden, J. Oomens, O. Dopfer, *J. Phys. Chem. A* 2010, 114, 13268; b) A. Lagutschenkov, J. Langer, G. Berden, J. Oomens, O. Dopfer, *Phys. Chem. Chem. Phys.* 2011, 13, 2815.

- [62] A. Lagutschenkov, O. Dopfer, *J. Mol. Spectrosc.* **2011**, *268*, 66.
- [63] S. Chakraborty, A. Patzer, O. Dopfer, *J. Chem. Phys.* **2010**, *133*, 440307.
- [64] J. Oomens, B. G. Sartakov, G. Meijer, G. von Helden, *Int. J. Mass Spectrom.* **2006**, *254*, 1.
- [65] S. Salzmänn, C. M. Marian, *Chem. Phys. Lett.* **2008**, *463*, 400.
- [66] P. R. Schreiner, A. A. Fokin, R. A. Pascal, A. de Meijere, *Org. Lett.* **2006**, *8*, 3635.
- [67] C. F. Correia, C. Clavaguera, U. Erlekam, D. Scuderi, G. Ohanessian, *ChemPhysChem* **2008**, *9*, 2564.
- [68] T. Zhang, K. Papson, R. Ochran, D. P. Ridge, *J. Chem. Phys. A* **2013**, *117*, 11136.
- [69] D. Oepts, A. F. G. van der Meer, P. W. van Amersfoort, *Infrared Phys. Technol.* **1995**, *36*, 297.
- [70] J. J. Valle, J. R. Eyler, J. Oomens, D. T. Moore, A. F. G. van der Meer, G. von Helden, G. Meijer, C. L. Hendrickson, A. G. Marshall, G. T. Blakney, *Rev. Sci. Instrum.* **2005**, *76*, 7.
- [71] A. Lagutschenkov, J. Langer, G. Berden, J. Oomens, O. Dopfer, *Phys. Chem. Chem. Phys.* **2011**, *13*, 15644.
- [72] Gaussian 03, M. J. Frisch, G. W. Trucks, H. B. Schlegel, G. E. Scuseria, M. A. Robb, J. R. Cheeseman, J. A. Montgomery, Jr., T. Vreven, K. N. Kudin, J. C. Burant, J. M. Millam, S. S. Iyengar, J. Tomasi, V. Barone, B. Mennucci, M. Cossi, G. Scalmani, N. Rega, G. A. Petersson, H. Nakatsuji, M. Hada, M. Ehara, K. Toyota, R. Fukuda, J. Hasegawa, M. Ishida, T. Nakajima, Y. Honda, O. Kitao, H. Nakai, M. Klene, X. Li, J. E. Knox, H. P. Hratchian, J. B. Cross, V. Bakken, C. Adamo, J. Jaramillo, R. Gomperts, R. E. Stratmann, O. Yazyev, A. J. Austin, R. Cammi, C. Pomelli, J. W. Ochterski, P. Y. Ayala, K. Morokuma, G. A. Voth, P. Salvador, J. J. Dannenberg, V. G. Zakrzewski, S. Dapprich, A. D. Daniels, M. C. Strain, O. Farkas, D. K. Malick, A. D. Rabuck, K. Raghavachari, J. B. Foresman, J. V. Ortiz, Q. Cui, A. G. Baboul, S. Clifford, J. Cioslowski, B. B. Stefanov, G. Liu, A. Liashenko, P. Piskorz, I. Komaromi, R. L. Martin, D. J. Fox, T. Keith, M. A. Al-Laham, C. Y. Peng, A. Nanayakkara, M. Challacombe, P. M. W. Gill, B. Johnson, W. Chen, M. W. Wong, C. Gonzalez, J. A. Pople, Gaussian, Inc., Wallingford CT, **2004**.
- [73] Avogadro: An Open-Source Molecular Builder and Visualization Tool. Version 1.01. <http://avogadro.openmolecules.net/>.
- [74] M. D. Wodrich, C. Corminboeuf, P. R. Schreiner, A. A. Fokin, P. v. R. Schleyer, *Org. Lett.* **2007**, *9*, 1851.

Received: March 18, 2014

Published online on June 4, 2014